Electronic Supplementary Material (ESI) for Journal of Materials Chemistry A.

Supporting Information

Integrated highly hydrated cellulose network with synergistic photothermal effect for efficient solar-driven water evaporation and salt resistance

Yu Chen, Jin Yang*, Lin Zhu, Xiaohua Jia, Sizhe Wang, Yong Li, Haojie Song*

School of Materials Science & Engineering, Shaanxi Key Laboratory of Green Preparation and Functionalization for Inorganic Materials, Shaanxi University of Science & Technology, Xi' an, Shaanxi, 710021, P.R. China

*Corresponding author: E-mail: yangjin@sust.edu.cn; songhaojie@sust.edu.cn

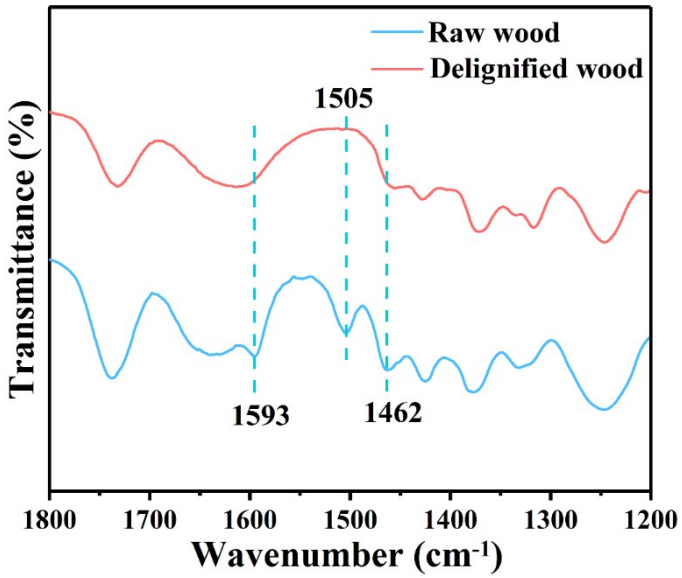

Fig. S1. ATR-FTIR spectra of raw wood and delignified wood. The characteristic peaks of lignin at 1593, 1505, and 1462 cm^{-1} (aromatic skeletal vibrations) disappeared after the chemical treatment.

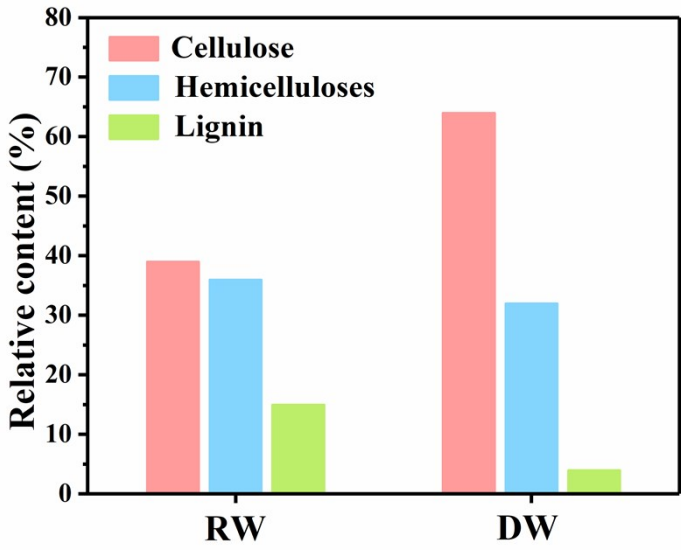

Fig. S2. Relative content of cellulose, hemicellulose, and lignin in cell walls of RW and DW.

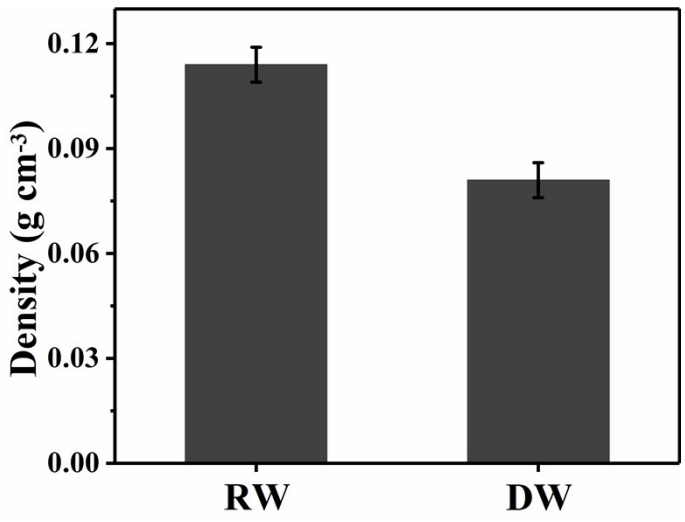

Fig. S3. The density of RW and DW.

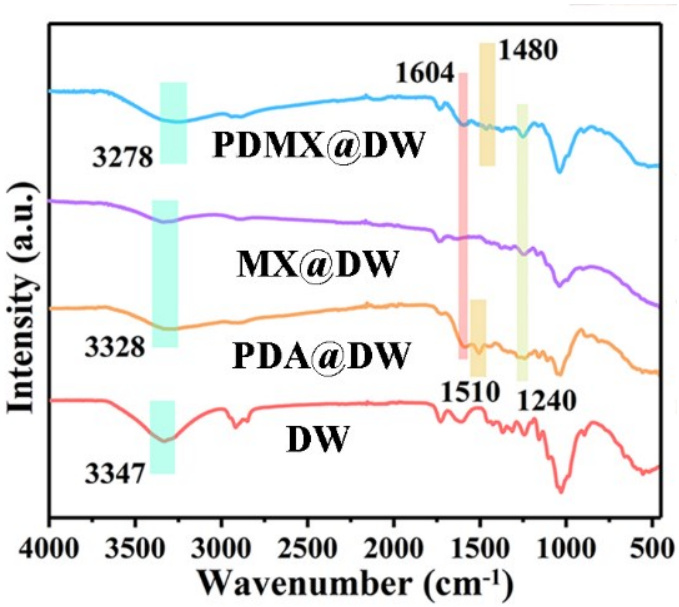

Fig. S4. ATR-FTIR spectra of DW, PDA@DW, MX@DW and PDMX@DW.

Compared to the DW sample, the stretching vibration of the O-H band shifts from 3347 cm^{-1} to 3328 cm^{-1}, which is attribute to the hydrogen bonding between the –OH functional groups of cellulose and the nitrogen lone pairs of PDA molecules. After the MX was transferred into the cellulose scaffold, the O–H peak (3328 cm^{-1}) shifted by 50 cm^{-1} with the extension of the impregnation time, indicating hydrogen bonds between MX and the cellulose nanofibrils. Meanwhile, the peaks of PDA@DW located at 1604, 1501, and 1240 cm^{-1} corresponds to –OH, C–H and C–N respectively, which indicates successful preparation of the PDA.

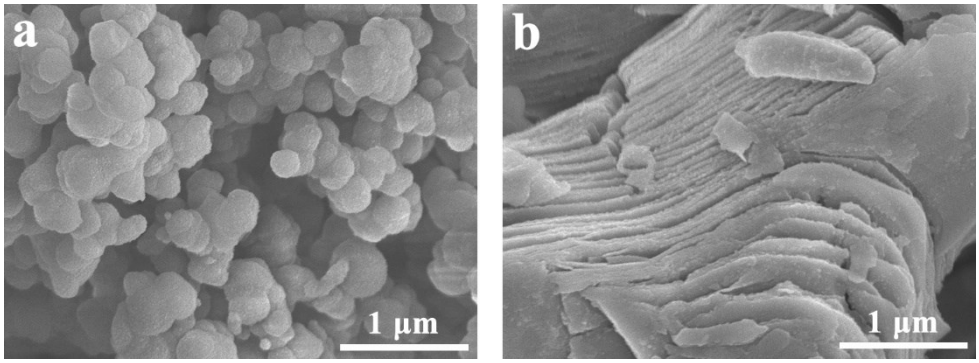

Fig. S5. SEM images of (a) pure PDA and (b) MX.

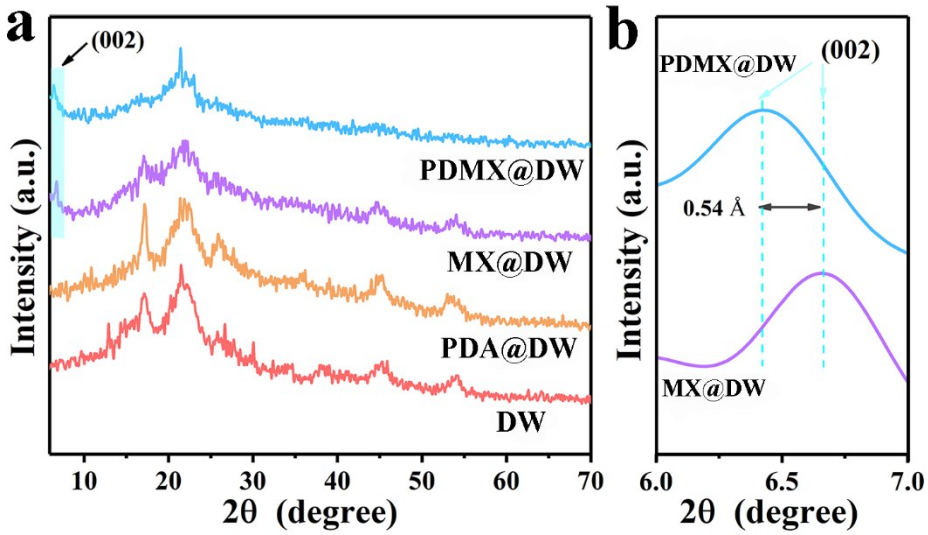

Fig. S6. XRD spectra of DW, PDA@DW, MX@DW, and PDMX@DW.

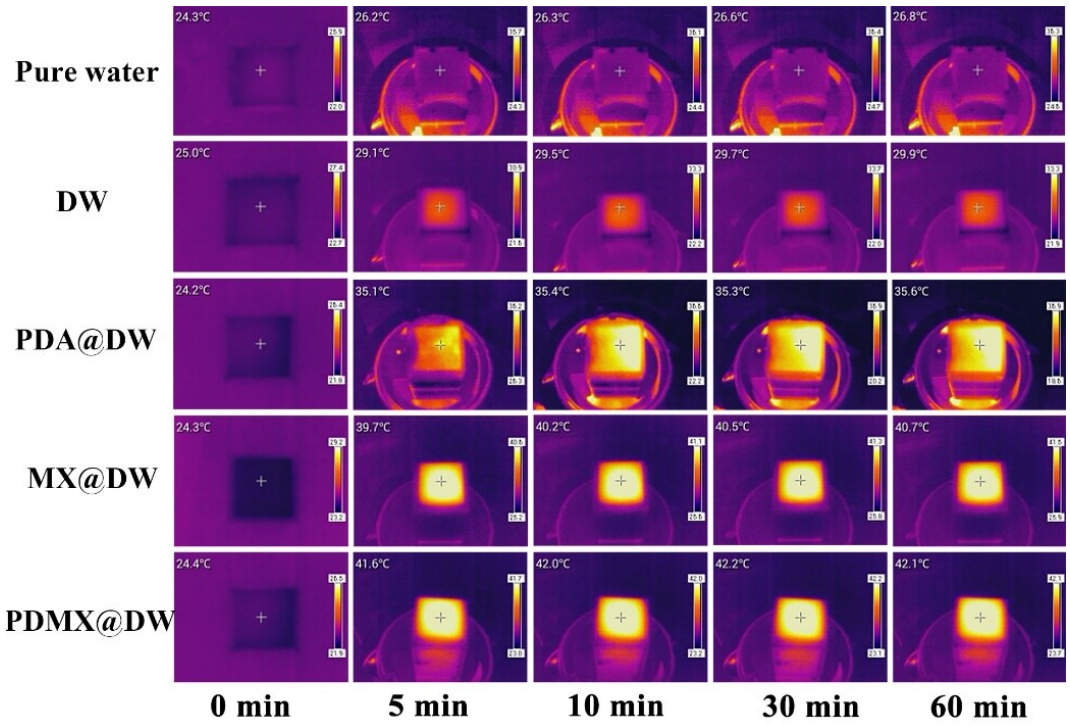

Fig. S7. The infrared thermal images of pure water, DW, PDA@DW, MX@DW, and PDMX@DW under 1 sun illumination within 1 h.

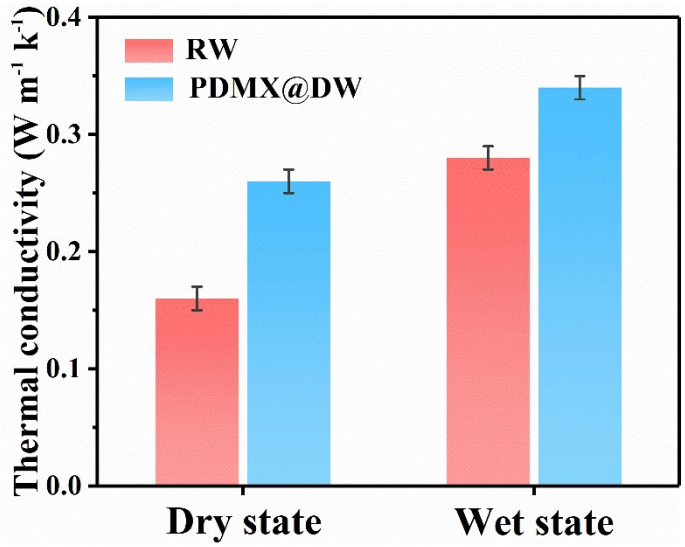

Fig. S8. Thermal conductivity of RW and PDMX@DW in dry and wet state.

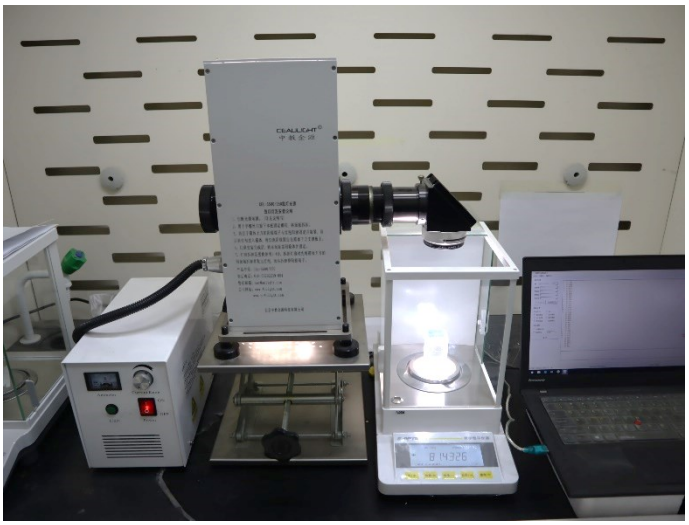

Fig. S9. The optical images of different aspects for solar–driven evaporation measurement platform.

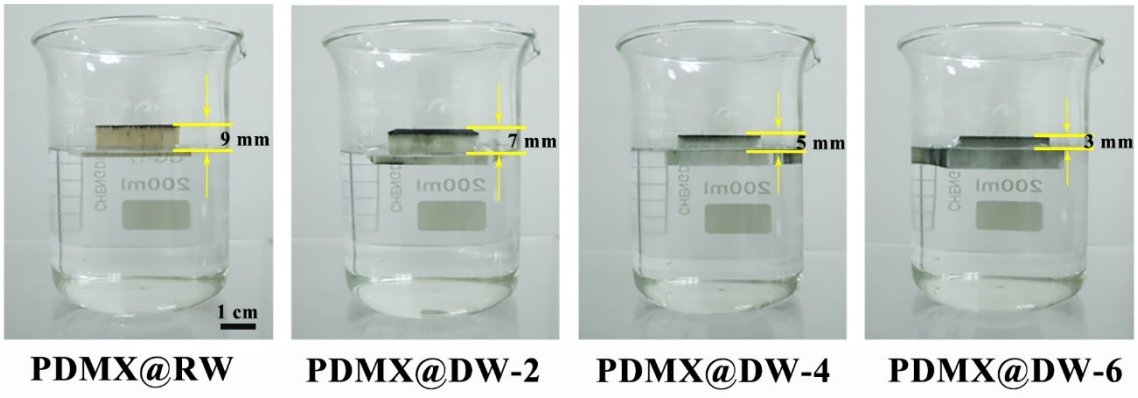

Fig. S10. The photos of different samples on the surface of pure water.

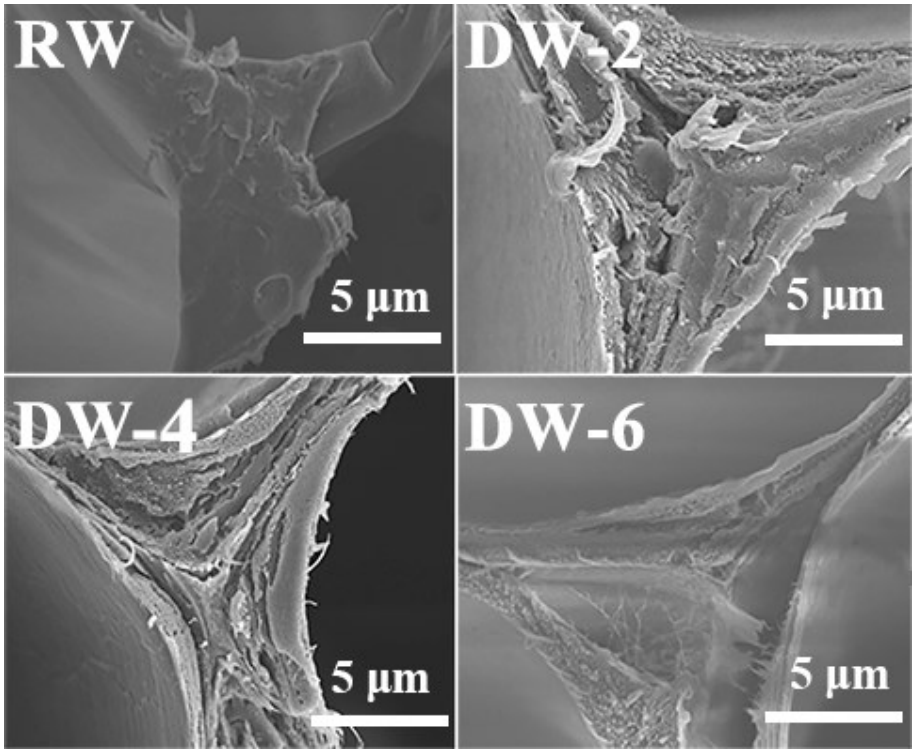

Fig. S11. SEM images of RW, DW-2, DW-4, and DW-6. As the delignification time increases, more cellulose is exposed. Especially for DW-6, the cellulose structure was even partially destroyed.

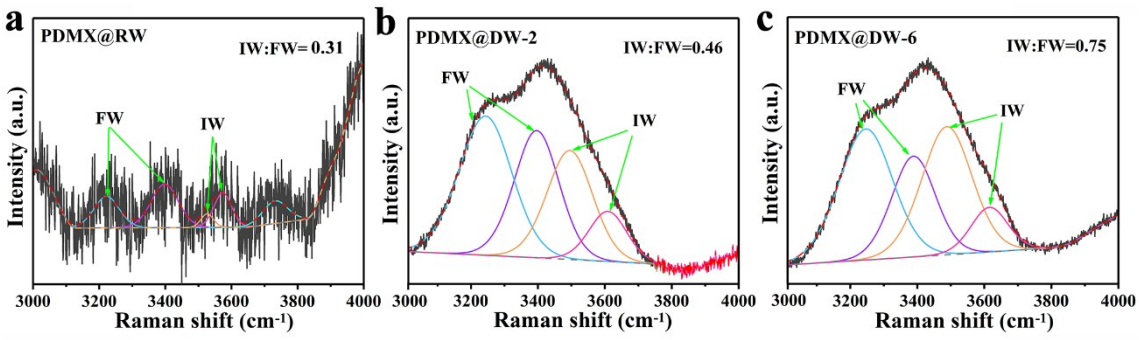

Fig. S12. Fitting curves in energy region of O-H stretching modes for PDMX@RW, PDMX@DW-2, and PDMX@DW-6.

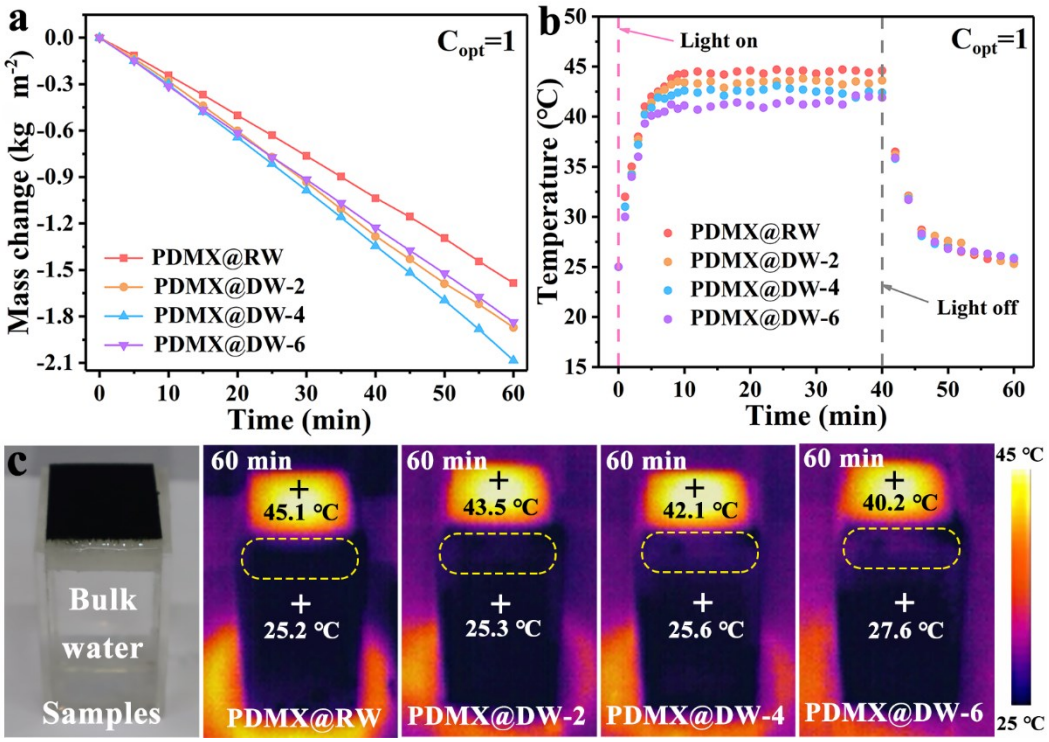

Fig. S13. **(a)** Mass change, and (b) surface temperature of PDMX@RW, PDMX@DW-2, PDMX@DW-4, and PDMX@DW-6, respectively. **(c)** The photograph of evaporation equipment, and corresponding IR images of different samples after 60 min of continuous exposure under 1 sun.

PDMX@DW-6 shows a low water evaporation rate (1.72 kg m^{-2} h^{-1}) (Fig. S13a). First, PDMX@DW-6 with higher hydrophilic will result in more water stored in the surface of evaporator. The heat of the photothermal layer is more likely to be dissipated into the bulk water, causing more heat loss and low surface temperature (Fig. S13b). Fig. S13c shows the overall temperature distribution of different evaporators after 60 minutes of continuous exposure to the sun. Obviously, the body water temperature of PDMX@DW-6 was increased to 27.6 °C, which may be the main source of the decrease in evaporation. On the other hand, it was observed on the SEM images of pure DW with different treatment time that RW, DW-2, and DW-4 showed a gradually clear cellulose

network (Fig. S11). For DW-6, the cellulose structure in the cell wall is destroyed, which may also be the reason for the reduced evaporation rate. Therefore, reasonably optimized saturated water content and cellulose network structure can effectively increase the evaporation rate of the evaporator.

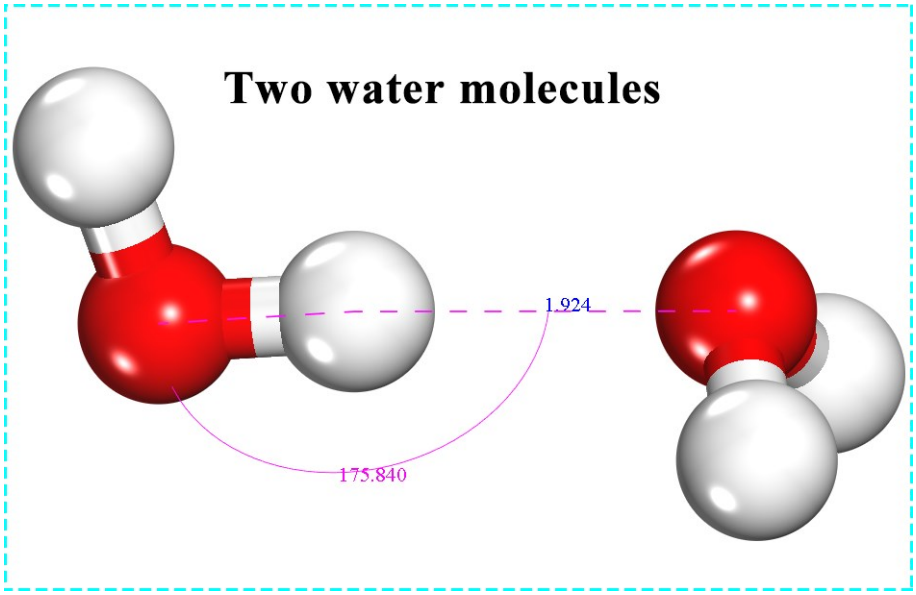

Fig. S14. The hydrogen bond length and angel of two water molecules.

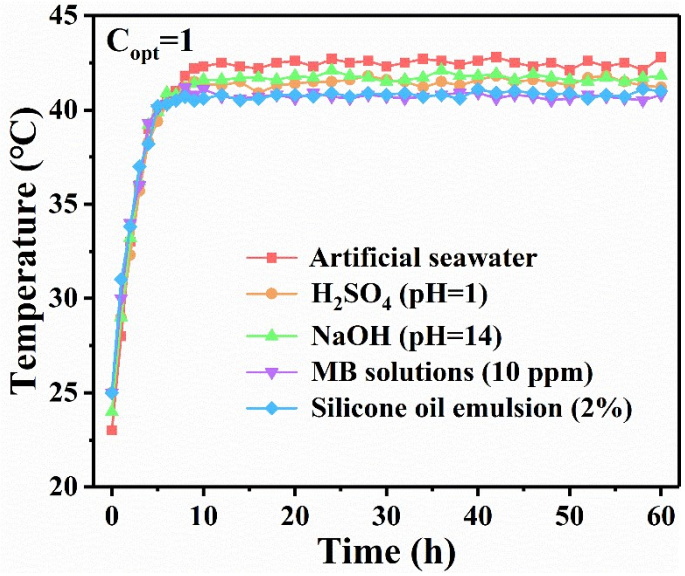

Fig. S15. The surface temperature of PDMX@DW in different types of solutions.

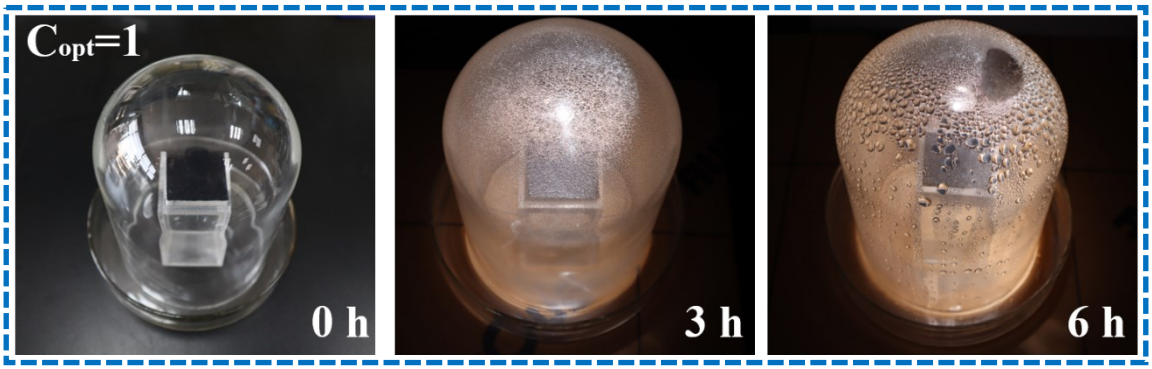

Fig. S16. The device of water collection.

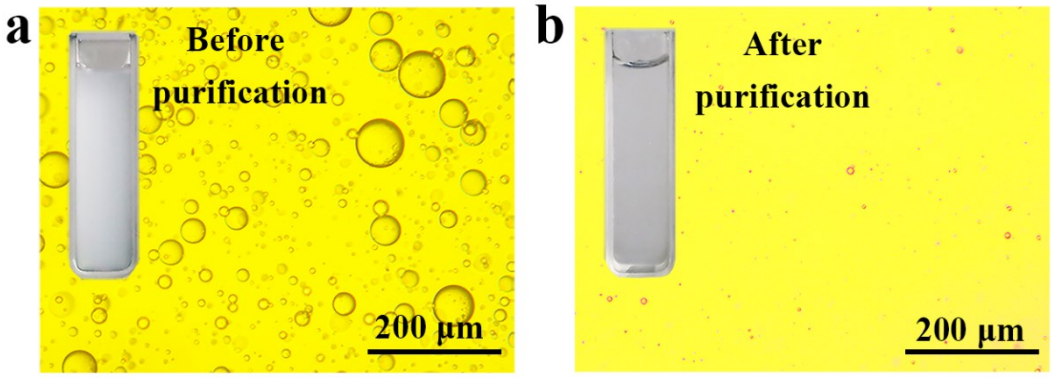

Fig. S17. The image of silicone oil emulsion before and after purification observed under an optical microscope.

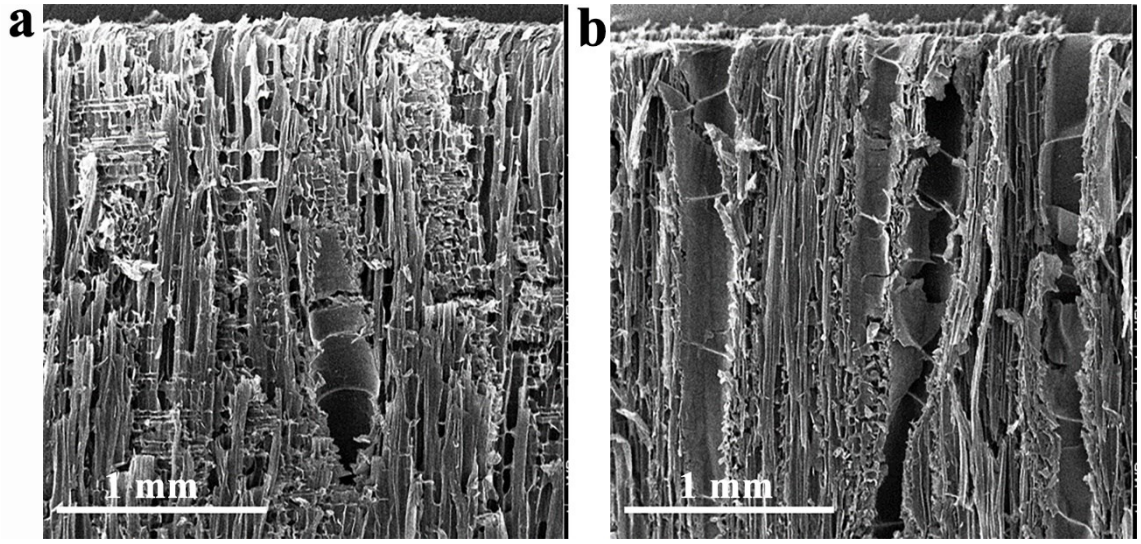

Fig. S18. SEM images of (a) PDMX@RW and (b) PDMX@DW side view.

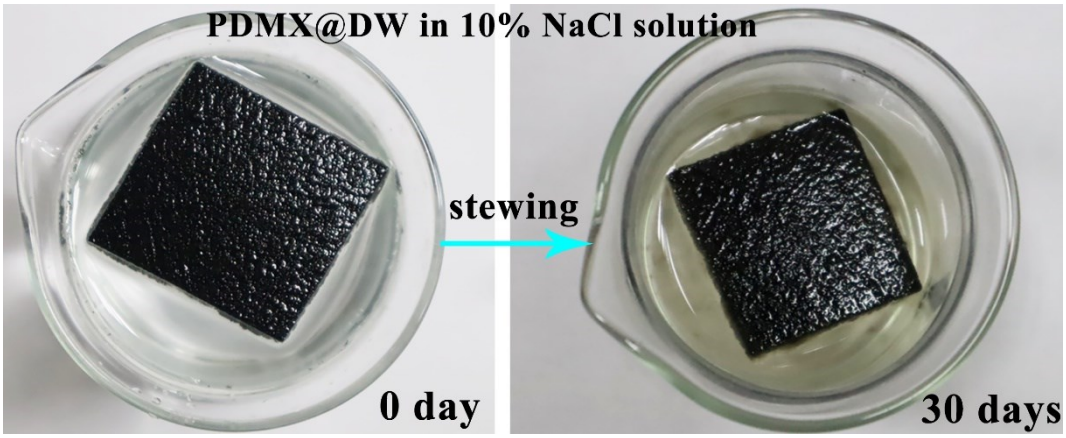

Fig. S19. PDMX@DW sample in 10% NaCl solution after 30 days.

Note S1

The conventional method for evaluating solar energy conversion efficiency (η) of solar desalination samples can be estimated by the following Equation:[1]

$$\eta = \nu(H_e + Q)/E_{in} \quad (1)$$

$$H_e = 1.91846 \times 10^6 [T / (T - 33.91]^2 \quad (2)$$

$$Q = c(T–T_1) \quad (3)$$

Here, ν corresponds to the evaporation rate of water (with the dark evaporation over the sample of 0.32 kg m^{-2} h^{-1} subtracted), H_e to the enthalpy change of the evaporation enthalpy of water passing from its liquid to gaseous phase, Q is the sensible heat per unit mass of water. E_{in} is incident light intensity of the simulated solar radiation, and c is the specific heat capacity of water, which measures approximately 4.2 J g $K^{–1}$, T_1 is the initial temperature of the water, T is the temperature of the evaporation process.

Calculation S1. The evaporation (photothermal conversion) efficiency of PDMX@DW.

Yu et al.[2] reported that the vaporization enthalpy of water in the polymer network structure is lower than that of bulk water (~2440 J/g). Following the previously reported work,[3, 4] we also conducted a control experiment to estimate the vaporization enthalpy of water in PDMX@DW. In detail, use two glassware with 3 × 3 × 6 cm as the container. One container is filled with water, and the other container is filled with PDMX@DW soaked in water. The two containers are placed in a constant temperature airtight box at the same time to avoid the influence of air convection on the evaporation

rate. The whole night experiment (more than 10 h) was carried out in a dark environment, and the mass loss of each glassware was recorded to estimate the solar evaporation rate. The above experiment was repeated six times and the evaporation rate were calculated, as shown in the table below.

Table S1:

Test	Room Temperature (℃)	Water Temperature (℃)	Evaporation rate of water (g m^{-2} h^{-1})	Evaporation rate of PDMX@DW (g m^{-2} h^{-1})	Evaporation rate ratio (water/ PDMX@DW)
1	24-26	20-22	89.6	115.9	0.7725
2	24-26	20-22	88.7	113.3	0.7829
3	24-26	20-22	94.4	125.5	0.7521
4	21-23	18-20	78.9	98.0	0.8048
5	21-23	18-20	73.4	92.4	0.7946
6	21-23	18-20	76.0	94.7	0.8019

To calculate the equivalent vaporization enthalpy of water in PDMX@DW, we hypothesized that under the same ambient temperature and pressure, the evaporation rate and vaporization enthalpy of pure water and PDMX@DW satisfy the following equation:[5, 6]

$$E_{PDMX@DW}M_{PDMX@DW}=E_{water}M_{water} \quad (4)$$

where $E_{PDMX@DW}$ and $M_{PDMX@DW}$ are the vaporization enthalpy and evaporation rate in PDMX@DW, E_{water} and M_{water} are the vaporization enthalpy and of pure water, respectively. Calculated based on the average of 6 tests, $M_{water}/M_{PDMX@DW}$ is about

0.7848. Using the reported vaporization enthalpy of pure water (~2440 J/g), the equivalent vaporization enthalpy of water in PDMX@DW can be calculated to be 1915 J/g based on the data in the above table. Thus, using the estimated enthalpy (1915 J/g) and the net evaporation rate of PDMX@DW, the photothermal efficiency of PDMX@DW under 1 sun is calculated to be 93.6%.

Table S2. Solar steam generation performance of PDMX@DW compared with other materials.

Sample	Temperature (℃)	Evaporation rate (kg m^{-2} h^{-1})	Efficiency (%)	Reference
Au nanoflowers gel	41.4	1.356	85.1	7
PDA-CA	40.0	1.36	86.0	8
MXene-based evaporator	35.5	1.393	93.4	9
Bridge-arched evaporator	46.2	1.476	92.9	10
CNTs@SiO_2 aerogels	34.0	1.50	91.6	11
TEMPO-PDA CM film	39.5	1.53	88.6	12
Ag-PDA@wood	45.2	1.56	88.7	13
Cellulose aerogels	35.1	1.82	95.0	14
Melamine sponges	45.1	1.98	92.0	4
PPy@MF	42.5	2.0	91.0	15
PDMX@DW	42.1	2.08	93.6	This work

Table S3. Comparison of vaporization enthalpy from DSC measurement and dark experiment.

Enthalpy (J/g)	Pure water	PDMX@RW	PDMX@DW-2	PDMX@DW-4	PDMX@DW-6
DSC measurement	2436	2409	2294	2096	2004
Dark experiment	2445	2374	2236	1915	1842

The DSC measured enthalpy of water is 2436 J/g, which is very close to the theoretical value of 2445 J/g, indicating the accuracy of our measurements. This enthalpy value for water in PDMX@DW-s is considerably higher than that estimated from the dark experiment discussed previously, due to the in DSC measurement being a complete dehydration process, whereby the water-polymer configuration changes significantly between a swelled state and a dehydrated state. For the dark experiment, weakly bonded water molecules in cellulose are constantly replenished through diffusion from the water reservoir, a process that more closely resembles that of the actual solar evaporation application.

References

1. X. Wu, E. R. Max, L. P. Jack, J. S. Tan, B. Shao, G. Owens, H. Xu, *Nano Energy*, 2019, **56**, 708-715.
2. Y. H. Guo, H. Y. Lu, F. Zhao, X. Y. Zhou, W. Shi, G. H. Yu, *Adv. Mater.*, 2020, **32**, 1907061.
3. F. Zhao, X. Y. Zhou, Y. Shi, X. Qian, M. Alexander, X. P. Zhao, S. Mendez, R. G. Yang, L. T. Qu, G. H. Yu, *Nat. Nanotechnol.*, 2018, **13**, 489.
4. F. Gong, H. L, W. B. Wang, J. G. Huang, D. W. Xia, J. X. Liao, M. Q. Wu, D. V. Papavassiliou, *Nano Energy*, 2019, **58**, 322-330.
5. L. Shi, Y. C. Wang, L. B. Zhang, P. Wang, *J. Mater. Chem. A*, 2017, **5**, 16212-16219.
6. P. P. Zhang, J. Li, L. X. Lv, Y. Zhao, L. T. Qu, ACS Nano, 2017, **11**, 5087-5093.
7. M. Gao, C. K. Peh, H. T. Phan, L. Zhu, G. W. Ho, *Adv. Energy Mater.*, 2018, **8**, 1800711.
8. Y. Zou, J. Y. Zhao, J. Y. Zhu, X. Y. Guo, P. Chen, G. G. Duan, X. H. Liu, Y. W. Li, *ACS Appl. Mater. Interfaces*, 2021, **13**, 7617−7624.
9. X. Q. Fan, Y. Yang, X. L. Shi, Y. Liu, H. P. Li, J. J. Liang, Y. S. Chen, *Adv. Funct. Mater.*, 2020, **30,** 2007110.
10. S. Meng, X. Zhao, C.-Y. Tang, P. Yu, R.-Y. Bao, Z.-Y. Liu, M.-B. Yang, W. Yang, *J. Mater. Chem. A*, 2020, **8**, 2701-2711.
11. X. Y. Dong, L. T. Cao, Y. Si, B. Ding, H. B. Deng, *Adv. Mater.*, 2020, **32**, 1908269.
12. Y. Zou, X. F. Chen, P. Yang, G. J. Liang, Y. Yang, Z. P. Gu, Y. W. Li, *Sci. Adv.*,

2020, **6**, eabb4696.

13. J. Yang, Y. Chen, X. H. Jia, Y. Li, S. Z. Wang, H. J. Song, *ACS Appl. Mater. Interfaces*, 2020, **12**, 47029-47037.
14. N. Li, L. F. Qiao, J. T. He, S. X. Wang, L. M. Yu, P. Murto, X. Y. Li, X. F. Xu, *Adv. Funct. Mater.*, 2020, **31**, 2008681.
15. J. X. Chen, B. Li, G. X. Hu, R. Aleisa, S. Lei, F. Yang, D. L. Liu, F. L. Lyu, M. Z. Wang, X. W. Ge, F. Qian, Q. Zhang, Y. D. Yin. *Nano Lett.*, 2020, **20**, 6051−6058.